Article

Chemistry & Biology

Nitric Oxide Synthase as a Target for Methicillin-Resistant *Staphylococcus aureus*

Graphical Abstract

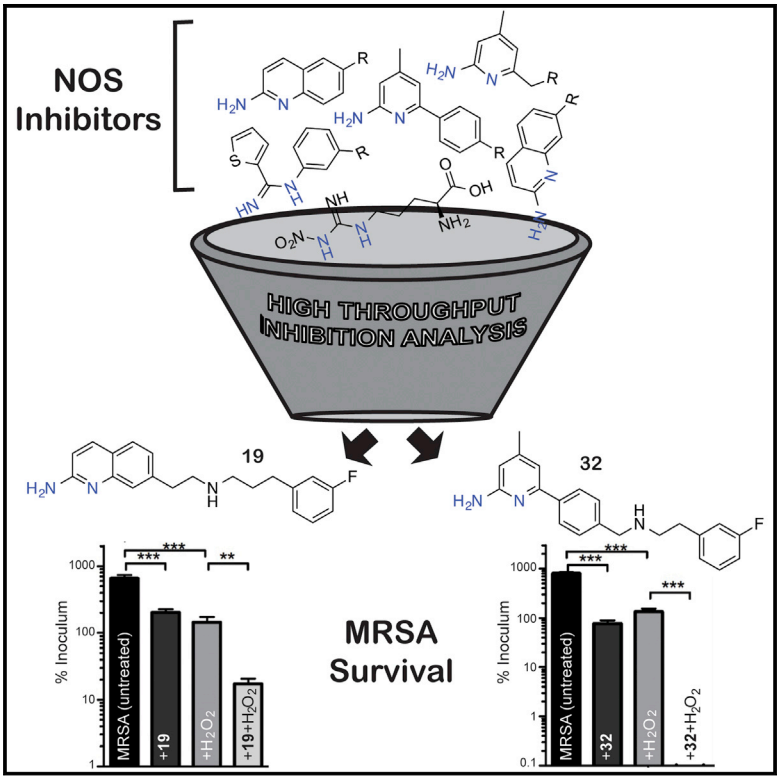

Authors

Jeffrey K. Holden, Soosung Kang, Federico C. Beasley, ..., Victor Nizet, Richard B. Silverman, Thomas L. Poulos

Correspondence

poulos@uci.edu (T.L.P.), agman@chem.northwestern.edu (R.B.S.)

In Brief

Holden et al. report on novel bacterial nitric oxide synthase (bNOS) inhibitors that work synergistically with agents that induce oxidative stress to dramatically inhibit the growth of methicillin-resistant *Staphylococcus aureus* (MRSA).

Highlights

- Inhibitors selective toward bacterial nitric oxide synthase have been identified
- These inhibitors are antimicrobial against MRSA
- Crystallography reveals the structural basis for selectivity
- NOS inhibitor library rapidly screened to identify potent inhibitors

Accession Numbers

4D7H
4D7I
4D7J
4D7O

Holden et al., 2015, Chemistry & Biology *22*, 785–792
June 18, 2015
http://dx.doi.org/10.1016/j.chembiol.2015.05.013

CellPress

Chemistry & Biology
Article

Nitric Oxide Synthase as a Target for Methicillin-Resistant *Staphylococcus aureus*

Jeffrey K. Holden,[1] Soosung Kang,[2] Federico C. Beasley,[3] Maris A. Cinelli,[2] Huiying Li,[1] Saurabh G. Roy,[4] Dillon Dejam,[1] Aimee L. Edinger,[4] Victor Nizet,[3] Richard B. Silverman,[2,*] and Thomas L. Poulos[1,*]
[1]Departments of Molecular Biology and Biochemistry, Pharmaceutical Sciences, and Chemistry, University of California, Irvine, CA 92697-3900, USA
[2]Departments of Chemistry and Molecular Biosciences, Chemistry of Life Processes Institute, Center for Molecular Innovation and Drug Discovery, Northwestern University, Evanston, IL 60208-3113, USA
[3]Departments of Pediatrics and Skaggs School of Pharmacy and Pharmaceutical Sciences, University of California, San Diego, CA 92093, USA
[4]Department of Developmental and Cell Biology, University of California, Irvine, CA 92697, USA
*Correspondence: poulos@uci.edu (T.L.P.), agman@chem.northwestern.edu (R.B.S.)
http://dx.doi.org/10.1016/j.chembiol.2015.05.013

SUMMARY

Bacterial infections associated with methicillin-resistant *Staphylococcus aureus* (MRSA) are a major economic burden to hospitals, and confer high rates of morbidity and mortality among those infected. Exploitation of novel therapeutic targets is thus necessary to combat this dangerous pathogen. Here, we report on the identification and characterization, including crystal structures, of two nitric oxide synthase (NOS) inhibitors that function as antimicrobials against MRSA. These data provide the first evidence that bacterial NOS (bNOS) inhibitors can work synergistically with oxidative stress to enhance MRSA killing. Crystal structures show that each inhibitor contacts an active site Ile residue in bNOS that is Val in the mammalian NOS isoforms. Mutagenesis studies show that the additional nonpolar contacts provided by the Ile in bNOS contribute to tighter binding toward the bacterial enzyme.

INTRODUCTION

As bacterial pathogens continually acquire resistance to commonly used antibiotics, it has become clear that novel therapeutic strategies are required to combat serious infections (Talbot et al., 2006). In particular, there is an urgent need for the development of new pharmaceuticals that target the pre-eminent Gram-positive human bacterial pathogen, methicillin-resistant *Staphylococcus aureus* (MRSA). MRSA, a Gram-positive pathogen resistant to common β-lactam antibiotics (Loomba et al., 2010), was first reported in 1961 (Jevons et al., 1961) and remains one of the most costly bacterial infections worldwide (Diekema et al., 2001). MRSA is a major threat to public health because of the high prevalence among nosocomial infections, and the emergence of highly virulent community-associated strains and their varying epidemiology (Stefani et al., 2012). In recent years, the threat of MRSA has been heightened by reports of strains resistant to vancomycin, as this agent is often considered the drug of last resort (Gardete and Tomasz, 2014). Characterization and exploitation of alternative bacterial drug targets will be essential for the future management of MRSA infections.

Recent gene deletion experiments in *S. aureus*, *Bacillus anthracis*, and *Bacillus subtilis* have implicated bacterial nitric oxide synthase (bNOS) as a potential drug target, since this enzyme provides the bacterial cell a protective defense mechanism against oxidative stress and select antibiotics (Gusarov et al., 2009; Shatalin et al., 2008; van Sorge et al., 2013). In Gram-positive pathogens, it has been proposed that bacterial NO functions to remove damaging peroxide species by activating catalase, and to limit damaging Fenton chemistry by nitrosylating thioredoxins involved in recycling the Fenton reaction (Gusarov and Nudler, 2005; Shatalin et al., 2008). We recently provided an initial proof of principle regarding pharmacological targeting of bNOS, as growth of the nonpathogenic model organism *B. subtilis* was severely perturbed in response to combination therapy with an active site NOS inhibitor and an established antimicrobial (Holden et al., 2013).

Design and development of a potent bNOS inhibitor against bone fide pathogens such as MRSA is complicated by the active site structural homology shared with the three mammalian NOS (mNOS) isoforms (Pant et al., 2002): neuronal NOS (nNOS), inducible NOS (iNOS), and endothelial NOS (eNOS). It is especially important not to inhibit eNOS given the critical role it plays in maintaining vascular tone and blood pressure (Yamamoto et al., 2001). Selectivity over nNOS may represent less of an immediate problem, since many of the polar NOS inhibitors characterized thus far are not very effective at crossing the blood-brain barrier (Silverman, 2009). Recent structure-based studies utilizing *B. subtilis* NOS (bsNOS) as a model system for bNOS suggest that specificity can be achieved through targeting the pterin binding site (Holden et al., 2013, 2014), as the bNOS and mNOS pterin binding sites are quite different.

To quickly identify potent bNOS inhibitors, we screened a diverse set of NOS inhibitors (Figure 1) using a novel chimeric enzyme recently reported for bNOS activity analysis (Holden et al., 2014). From this high-throughput analysis we were able to identify two potent and chemically distinct bNOS inhibitors.

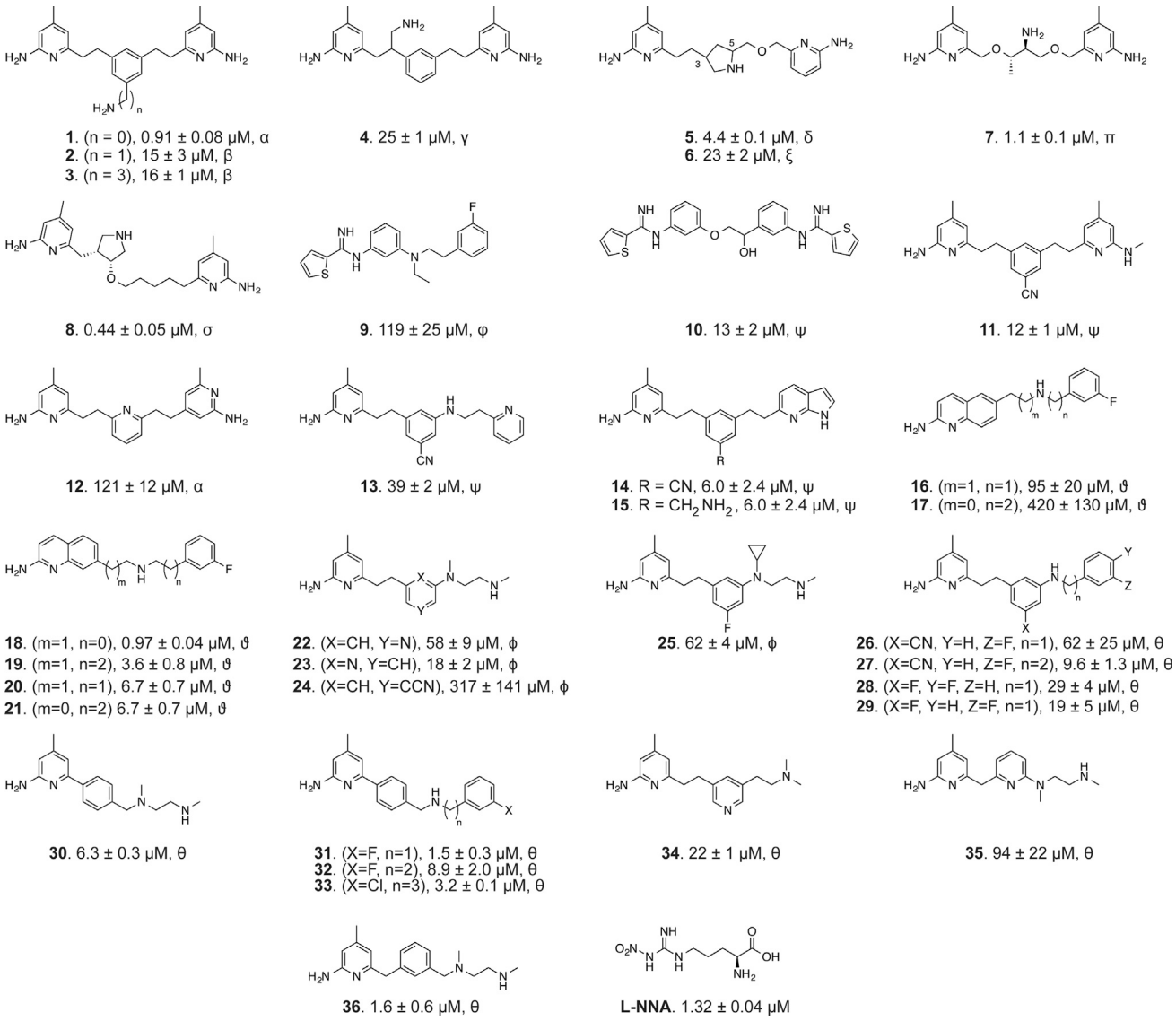

Figure 1. NOS Inhibitor Library Used in this Study

The inhibitor K_S values, determined from an imidazole displacement assay, are reported in μM for each inhibitor of bsNOS. Isolation and characterization of NOS inhibitors marked by α were previously reported by Delker et al. (2010), β by Huang et al. (2013), γ by Huang et al. (2014), δ by Holden et al. (2013), ξ by Jing et al. (2014), π by Holden et al. (2013), σ by Huang et al. (2012), φ by Huang et al. (2014), ψ by Holden et al. (2014), ϑ by Cinelli et al. (2014), and ϕ by K.S. (unpublished data); inhibitors marked by θ are reported in this article.

Crystal structures and binding analyses of these inhibitors revealed both to bind a hydrophobic patch within the bNOS active site. Moreover, both compounds possess antimicrobial activity against *S. aureus*, suggesting that these NOS inhibitors could represent viable new drug leads against this foremost human pathogen so frequently resistant to current antimicrobials.

RESULTS AND DISCUSSION

Identification of Potent bNOS Inhibitors

Rapid identification of molecular fragments that function as potent bNOS inhibitors is a key initial step toward the design and characterization of future bNOS inhibitors. To carry this out, we adapted a bNOS activity assay (Holden et al., 2014) to screen through a series of NOS inhibitors using a single time-point approach (Figure 2). Concurrently, we measured the K_S for each inhibitor using the imidazole displacement assay. In both of these studies bsNOS was used as a model system, since bsNOS assays are well developed and bsNOS shares high active site sequence homology with *S. aureus* and *B. anthracis* NOS enzymes. While all inhibitors bound to bsNOS in the μM range, the most potent bsNOS inhibitors identified from the activity analysis were calculated to have K_S values in the low-μM to nM range. Using the single time-point approach in combination with the imidazole displacement assay, we identified compounds that were both potent inhibitors and tight binders to the active site.

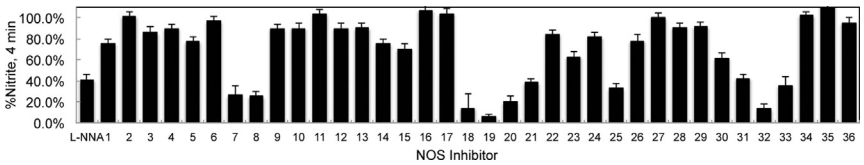

Figure 2. Based on a Single Time-Point Analysis Using bBiDomain to Evaluate Bacterial NOS Inhibition, NOS Inhibitors Have Varying Potency Toward Bacterial NOS

Nitrite concentrations were measured after a 4-min incubation. Error bars represent the average ± SEM for three separate experiments.

Since N^G-nitro-L-arginine (L-NNA) is an excellent inhibitor analog of the NOS substrate L-Arg, the potency of L-NNA at 40.9% ± 5.3% nitrite (Figure 2) was established as an arbitrary threshold for identifying designer molecules with increased potency. Using L-NNA as a benchmark led us to classify several NOS inhibitors as potent bNOS inhibitors. This group includes three aminoquinoline inhibitors, two 6-benzyl-aminopyridine inhibitors, and two aminopyridine inhibitors. Of the two aminopyridine inhibitors, **7** was previously described as a NOS inhibitor with antimicrobial properties (Holden et al., 2013). Since we previously characterized the binding of aminopyridine inhibitors to bsNOS, we selected the most potent aminoquinoline and 6-benzyl-aminopyridine-based inhibitors, **19** and **32**, respectively, for further analysis. Compounds **19** and **32** were also the two most potent inhibitors of the 37 NOS inhibitors evaluated using the bsNOS single time-point analysis at 6.1% nitrite and 13.2% nitrite, respectively. In addition, inhibitor potency of **19** and **32** was a direct result of competing with substrate at the active site, as neither compound influenced electron transfer rates or the Griess reaction chemistry used to measure bNOS activity (Figure S1; Table S1).

Isoform Selectivity of NOS Inhibitors

Compounds **19** and **32** were next assayed separately against purified NOS isoforms at varying concentrations (Holden et al., 2014). Even though the median inhibitory concentration (IC_{50}) for both mNOS and bsNOS was measured by complementary methods, both methods allowed for an excellent comparison of inhibitor potency, as the IC_{50} was used to calculate K_i using the Cheng-Prusoff equation (Cheng and Prusoff, 1973). From our K_i analysis (Table 1), it is clear that both **19** (269 nM) and **32** (1940 nM) function as potent bNOS inhibitors and demonstrate excellent selectivity over both iNOS and eNOS (Table 1). Although selectivity over nNOS remains an issue, it is unclear whether cross-reactivity with nNOS expressed in neuronal tissues would represent an important limiting factor for these drugs during short-course antibacterial therapy unless blood-brain penetration was high; indeed, nNOS inhibition itself has been examined as a treatment for Parkinson's disease in a rat model (Yuste et al., 2012).

To better understand the structural basis for inhibitor potency and selectivity, we solved inhibitor bound crystal structures of **19** and **32** (Figure 3; Table 2). Both **19** and **32** were co-crystallized in the presence of the pterin molecule H_4B. However, the physiological pterin group for bNOS remains unclear, as many bNOS-containing bacteria do not contain the biosynthetic machinery required for H_4B synthesis (Pant et al., 2002). Previous work showed the ubiquitous pterin, tetrahydrofolate, supports NO production by bNOS (Adak et al., 2002; Reece et al., 2009). In NOS crystal structures, H_4B binding is stabilized by an H bond to heme propionate D, an H bond with a conserved Arg residue, and a π-π stacking interaction with a conserved Trp residue (Figure 3). Although the function of pterins in bNOS is unclear, spectroscopic studies indicate that pterins are not required for stability, as in mNOS; pterins are required for electron transfer in all NOS isoforms (Chartier and Couture, 2004).

Although **19** and **32** are chemically quite different, they both bind to the active site Glu-243 through a series of H bonds, and do not interact with H_4B. For the nNOS inhibitor bound crystal structures, the fluorinated-benzyl group of both **19** and **32** bound to a hydrophobic pocket adjacent to the heme propionate group. This hydrophobic pocket is composed of residues Leu-337 and Met-336 from the N-terminal Zn^{2+} binding motif and Tyr-706 (Figures 3A and 3B). Unlike nNOS, bNOS does not contain an N-terminal Zn^{2+} binding motif, and therefore does not contain an analogous hydrophobic pocket adjacent to the heme propionate. Despite slight differences in binding of the fluorinated-benzyl group, in both NOS isoforms the binding of **19** and **32** was further stabilized by H bonds between the secondary amine of each inhibitor and the heme propionate groups (Figures 3D and 3E). Direct comparison of the bsNOS-**19** and the previously reported nNOS-**19** (Cinelli et al., 2014) structures revealed the binding mode of **19** to be unchanged between the two NOS isoforms. However, the binding mode in bsNOS was further stabilized by the hydrophobic contact between Ile-218 and the aminoquinoline group of **19**. Since Ile-218 is within van der Waals contact of **19** and the analogous residue in nNOS is Val-567, our data suggest that the slight differences in hydrophobicity between Ile and Val allow for improved binding of **19** to bsNOS.

Similar to **19**, crystal structure analysis of **32** demonstrates the inhibitor binding mode to be further stabilized by the hydrophobic contact between the inhibitor and Ile-218 (Figure 3C; Figure S1). In both the nNOS-**32** and I218V-bsNOS-**32** crystal structures (Figures 3E and 3F, respectively), the inhibitor binding mode of **32** is unchanged by the Ile/Val difference, compared with wild-type (WT) bsNOS. To evaluate the contribution of Ile-218 to the inhibitor binding mode, we measured inhibitor binding using the imidazole displacement assay. From this analysis we found the inhibitor binding of both **19** and **32** to be ~5- to 6-fold tighter to Ile-218 over I218V (Table 3). The crystal structures and binding assay results suggest that the increased

Table 1. Inhibition of NOS Isoforms by Inhibitors 32 and 19

Inhibitor	K_i bBiDomain (nM)	K_i nNOS (nM)	K_i iNOS (nM)	K_i eNOS (nM)
19	269	164	31,900	7,250
32	1,940	525	6,440	2,870

The bBiDomain construct was used to evaluate inhibitor K_i against bsNOS.

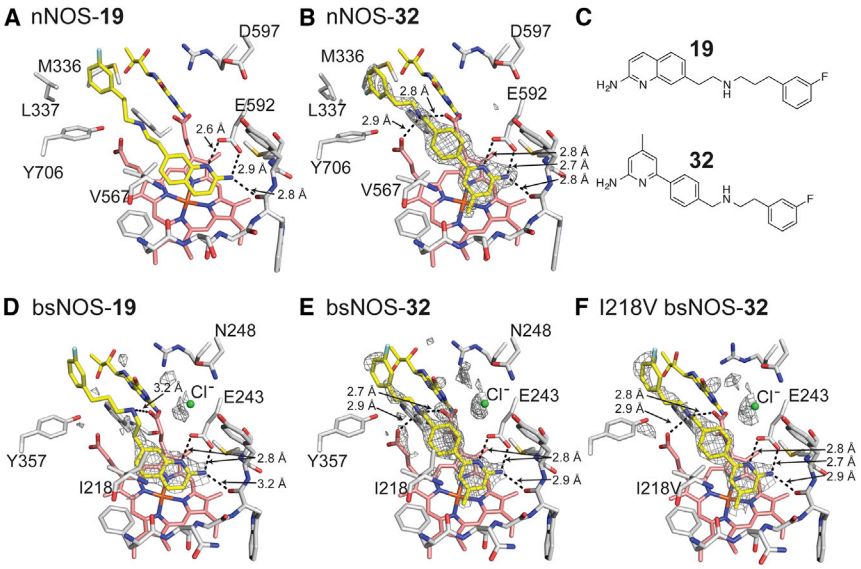

Figure 3. Inhibitor Bound NOS Crystal Structures with Select Side Chains Colored White, Heme Group Colored Salmon, and Both the Active Site Inhibitor and H_4B Molecule Colored Yellow

For bsNOS inhibitor bound structures there is a chlorine ion bound at the carboxylate binding site of L-Arg, which is shown as a green sphere. Both **19** and **32** bind to nNOS and bsNOS. In the nNOS structures (A and B) the fluorinated-benzyl group binds to a hydrophobic patch that is not present in bsNOS, adjacent to the heme propionate and composed of Y706, L337, and M336. At the NOS active sites, both **19** and **32** bind in similar orientations to form a network of H bonds indicated by dashed lines. For the bsNOS structures, both **19** and **32** are within a hydrophobic contact of bsNOS I218.

(A) **19** bound to nNOS (PDB: 4CAO).

(B) **32** bound to nNOS with the F_O-F_C map contoured at 4.0σ.

(C) Chemical representations of **19** and **32**.

(D) **19** bound to bsNOS with the F_O-F_C map contoured at 3.0σ.

(E) **32** bound to bsNOS with the F_O-F_C map contoured at 3.0σ.

(F) **32** bound to I218V bsNOS with the F_O-F_C map contoured at 3.0σ.

hydrophobicity of Ile-218 over the analogous mNOS Val residue improves inhibitor binding to bNOS. This is partly observed in the crystal structures, as binding of **19** or **32** induces an alternative rotameric position in Ile-218 to form a hydrophobic contact with both **19** and **32** (Figure S1). Considering that Ile-218 is conserved across all bNOS enzymes (Wang et al., 2004), future inhibitors designed to target bNOS should continue to exploit Ile-218 by using the scaffolds of **19** and **32**.

Anti-MRSA Activity of NOS Inhibitors

To evaluate the antibacterial potential of NOS inhibitors **19** and **32** on bacterial growth, we utilized the highly virulent CA-MRSA strain UAMS118 (*wt*) representative of the USA300 clonal lineage and a previously engineered isogenic NOS deletion mutant (van Sorge et al., 2013). Since previous experiments have shown bacterial *Δnos* strains are more susceptible to H_2O_2-mediated killing (Holden et al., 2013; Shatalin et al., 2008; van Sorge et al., 2013), we measured the effect of NOS inhibitors and H_2O_2 on *S. aureus* (Figure 4). Our results both confirm that the *Δnos* strain is more susceptible to H_2O_2-mediated killing than the *wt* strain, and further demonstrate that co-treatment of *S. aureus* with H_2O_2 and a NOS inhibitor significantly increases the H_2O_2-mediated killing of the bacteria. Interestingly, both **19** and **32** exhibit some direct bacteria toxicity at 200 μM, as demonstrated by the modest decrease in bacterial survival for both *wt* and *Δnos* when treated with inhibitor alone (Figure 4). For example, at 60 min **19** alone decreases growth by about 3-fold, but with peroxide **19** decreases growth 30-fold. While this indicates a modest effect on non-NOS targets, the primary effect of **19** is to impart far greater sensitivity to oxidative stress, and is consistent with **19** operating primarily by inhibiting bNOS. We also evaluated the toxicity of **19** and **32** using mouse embryonic fibroblast cells and found the IC_{50} values for **19** and **32** to be 5.84 μM and 11.86 μM (Table S2), respectively. These data indicate that toxicity of NOS inhibitors toward mammalian cells needs to be lowered for further consideration as a therapeutic agent.

The major effect of **19** and **32** is to work synergistically with H_2O_2 to significantly limit bacterial growth, most likely by limiting NO production. These results are consistent with previous results indicating that blocking of NO signaling increases bacterial susceptibility to oxidative stress (Gusarov and Nudler, 2005; Holden et al., 2013), and indicate that **19** and **32** could perhaps function as antimicrobials to increase susceptibility to innate immune clearance via an oxidative burst. Furthermore, considering that many existing pharmaceutical antibiotics function through an oxidative mechanism (Kohanski et al., 2007), bNOS inhibitors such as **19** and **32** could theoretically synergize to increase the killing efficiency of such agents.

SIGNIFICANCE

NO generated by bNOS helps to protect certain Gram-positive bacteria from oxidative stress, including antibiotic-induced oxidative stress (Gusarov and Nudler, 2005; Gusarov et al., 2009; van Sorge et al., 2013). In earlier work, we found that a small number of inhibitors developed for selective nNOS inhibition also improved the efficacy of antimicrobials, suggesting that bNOS might be a viable drug target (Holden et al., 2013). In the present study we sought to achieve two goals. The first was to identify bNOS-selective inhibitors with antimicrobial activity against the important human pathogen, MRSA. Of the many compounds screened, two were found to bind well to bNOS and exhibit antimicrobial activity with selectivity over eNOS and iNOS. Selectivity over eNOS is more important, since interfering with eNOS will adversely affect the critical role that

Table 2. Data Collection, Processing, and Refinement Statistics of the NOS Inhibitor Bound Structures

	bsNOS-**19**	bsNOS-**32**	I218V bsNOS-**32**	nNOS-**32**
	PDB: 4D7H	PDB: 4D7J	PDB: 4D7I	PDB: 4D7O
Data Collection				
Wavelength (Å)	0.976484	0.918370	0.999746	0.9999
Space group	$P2_12_12$	$P2_12_12$	$P2_12_12$	$P2_12_12_1$
No. of unique reflections	32,128 (2,261)	70,341 (3,408)	48,394 (2,575)	90,851 (3,910)
Cell dimensions				
a, *b*, *c* (Å)	80.9, 94.7, 62.8	80.5, 94.8, 62.8	80.6, 95.0, 61.6	51.8, 110.6, 165.2
α, β, γ (°)	90, 90, 90	90, 90, 90	90, 90, 90	90, 90, 90
Resolution (Å)	49.62–2.02 (2.07–2.02)[a]	37.06–1.55 (1.58–1.55)[a]	48.94–1.96 (2.01–1.96)[a]	1.78 (1.81–1.73)
R_{merge}	0.128 (0.570)	0.052 (2.522)	0.135 (1.518)	0.061 (0.662)
R_{PIM}	0.078 (0.530)	0.033 (1.599)	0.096 (1.074)	0.030 (0.385)
$CC_{1/2}$	0.997 (0.834)	1.000 (0.528)	0.992 (0.558)	0.999 (0.834)
$I/\sigma I$	10.1 (1.6)	18.0 (0.6)	7.3 (1.0)	26.4 (1.2)
Completeness (%)	99.5 (97.5)	99.8 (99.8)	99.6 (100.0)	99.0 (87.1)
Redundancy	5.2 (3.0)	6.5 (6.7)	4.3 (4.4)	4.9 (3.3)
Refinement				
Resolution (Å)	49.62–2.02 (2.092–2.02)	37.061–1.550 (1.605–1.55)	48.94–1.96 (2.03–1.96)	92.07–1.78 (1.826–1.78)
No. of reflections used	31,936	70,050	34,419	90,785
Completeness (%)	98.8	99.45	99.23	98.86
R_{work}	0.1849 (0.2734)	0.173 (0.3612)	0.1893 (0.3501)	0.1794 (0.289)
R_{free}	0.2377 (0.3350)	0.2035 (0.3715)	0.2352 (0.3622)	0.2092 (0.294)
No. of atoms				
Total	3,257	3,468	3,253	7,283
Macromolecules	2,952	2,950	2,940	6,673
Ligands	101	121	92	179
Solvent	204	397	221	431
B factor				
Average	41.4	28.7	41.1	38.1
Macromolecules	41.4	27.7	41.2	38.5
Ligands	42.8	29.5	34.5	26.1
Solvent	41.9	36.4	42.9	38
Root-mean-square deviations				
Bond lengths (Å)	0.007	0.007	0.008	0.01
Bond angles (°)	1.177	1.195	1.19	1.311

[a]Values in parentheses are for highest-resolution shell.

eNOS-derived NO plays in maintaining vascular tone and blood pressure (Yamamoto et al., 2001). The second goal was to use crystallography to identify subtle differences between the bNOS and mNOS active sites to exploit for future inhibitor design. Ile-218 (Val in mNOS) contacts the inhibitors, and the I218V mutant exhibits about a 6-fold lower affinity than WT. Although this is a rather modest difference, we have also found that several NOS inhibitors more readily bind to the pterin site in bNOS (Holden et al., 2015). Given the lower affinity of pterins for bNOS compared with mNOS, this is another important binding site difference between bNOS and mNOS. The Ile versus Val active site difference, together with the larger structural differences in the pterin site, are critical molecular features that could be exploited in future inhibitor design efforts.

EXPERIMENTAL PROCEDURES

Molecular Biology

Active site mutation I218V was introduced to bsNOS by site-directed mutagenesis using PfuTrubo (Agilent). Both WT and I218V bsNOS were expressed and purified from *Escherichia coli* as previously described for bsNOS (Pant et al., 2002). YumC and bBiDomain were also purified from *E. coli* and used for activity analysis (Holden et al., 2014). Recombinant rat nNOS and murine iNOS were expressed in *E. coli* and isolated as reported previously (Hevel et al., 1991; Roman et al., 1995).

Bacterial NOS Activity Inhibition

Reactions containing both bBiDomain (a chimera of bsNOS and redox partner YkuN) and YumC were initiated with reduced nicotinamide adenine dinucleotide phosphate (NADPH) and run for 4 min at 35°C as previously described (Holden et al., 2014). Substrate *N*-ω-hydroxy-L-arginine (NOHA) and NOS inhibitor were included in each reaction at 200 and 30 μM, respectively. The

Table 3. Calculated K_S Values by Imidazole Displacement for NOS Ligands to bsNOS

Ligand	WT K_S (μM)	I218V K_S (μM)
L-Arg	4.8 ± 0.1 (Wang et al., 2004)	2.0 ± 0.2 (Wang et al., 2004)
19	3.6 ± 0.8	18 ± 2
32	8.9 ± 2.0	58 ± 4

Griess reaction was used to measure nitrite levels as a function of NOS activity. Percentage of nitrite was calculated for each reaction as the concentration of nitrite detected in the presence of inhibitor divided by the concentration of nitrite detected without inhibitor present. Each reaction was measured in duplicate for three separate trials.

K_i Determination

The K_i was calculated from the half-maximal inhibitor concentration (IC_{50}) and K_D of L-NOHA using the Cheng-Prusoff equation (Cheng and Prusoff, 1973). For bBiDomain, the previously reported K_D of L-NOHA at 23.5 μM (Hannibal et al., 2011) was used to calculate K_i. IC_{50} was measured for bsNOS using bBiDomain and YumC as previously described (Holden et al., 2014). Cross-reactivity of inhibitors **19** and **32** was checked over a concentration range of 0.01–50 μM inhibitor with the Griess reagents, and neither compound interfered or contributed toward the Griess reaction. IC_{50} for mammalian NOS was determined using the oxyhemoglobin assay as previously described (Huang et al., 2014).

Cytochrome *c* Oxidase Activity

Horse heart cytochrome *c* oxidase reduction was evaluated as previously described (Holden et al., 2014) using $\Delta\varepsilon_{550}$ = 21 mM^{-1} cm^{-1} (Martasek et al., 1999) and NADPH at 100 nM to initiate the reaction. For individual reactions containing a NOS inhibitor, inhibitor concentrations were set at 1 μM, 10 μM, and 50 μM inhibitor. Each reaction contained bBiDomain and YumC at 100 nM and 1 μM, respectively.

Crystallization and Structure Determination

Although the target of this study is *S. aureus*, we utilized bsNOS owing to the better diffraction power of bsNOS crystals. In fact, bsNOS and *S. aureus* NOS (saNOS) (Bird et al., 2002) are very similar, and the crystal structures superimpose with a 0.55-Å root-mean-square deviation of α carbon atoms. In addition, 32 of 33 residues within 10 Å of the heme iron and 14 of 17 residues within 10 Å of the pterin cofactor are identical. As a result, structural insights gained from bsNOS are directly applicable to saNOS. Crystals of bsNOS and the I218V mutant were prepared using the hanging-drop method by mixing protein at 18 mg/ml and well solution in a 1:1 ratio. Prior to crystallization, the protein was stored in a buffer composed of 25 mM Bis-Tris methane at pH 7.4, 75 mM NaCl, 2% (v/v) glycerol, 0.5% (w/v) PEG3350, and 1 mM DTT. The well solution used for crystallization was composed of 60 mM Bis-Tris methane, 40 mM citric acid, 15% (w/v) PEG3350, and 1.9% (v/v) 1-propanol at pH 7.6. Crystals grew overnight after seeding with old crystals. Crystals were cryoprotected in the well solution supplemented with 30% (v/v) glycerol, 2 mM H_4B, and 5–10 mM inhibitor prior to being flash-frozen at 100 K. Crystals of rat nNOS oxygenase domain were prepared and flash-frozen as previously described (Li et al., 2014). Data were collected under cryogenic conditions on individual crystals at both the Advanced Light Source (Berkeley, CA) and Stanford Synchrotron Radiation Lightsource (Menlo Park, CA). The raw data frames were indexed and integrated using either iMOSFLM (Battye et al., 2011) or XDS (Kabsch, 2010). The program Aimless was then used to scale the datasets (Evans, 2006). Inhibitor bound structures were refined using either PHENIX (Adams et al., 2009) or Refmac (Vagin et al., 2004), with inhibitor restraints built using PRODRG (Schuttelkopf and van Aalten, 2004).

Imidazole Displacement

Purified bsNOS was diluted to 2 μM into a buffered solution containing 50 mM Tris (pH 7.6), 10 mM NaCl, 100 μM DTT, and 1 mM imidazole to generate a low-spin heme. NOS inhibitors were titrated into the bsNOS-buffered solution, and the conversion of the heme group from low spin to high spin was monitored using a Cary 3E UV-visible spectrophotometer. The K_S was calculated as previously described from the $K_{S,app}$ (Holden et al., 2013; Roman et al., 1995) using the bsNOS K_D imidazole at 384 μM and the bsNOS-I218V K_D imidazole at 506 μM (Wang et al., 2004).

Effect of Antimicrobial-Induced Stress and NOS Inhibitors on *S. aureus*

Creation of the *S. aureus* UAMS1182 *nos* isogenic knockout is described in a previous report (van Sorge et al., 2013). Parent (WT, *wt*) and knockout (Δ*nos*)

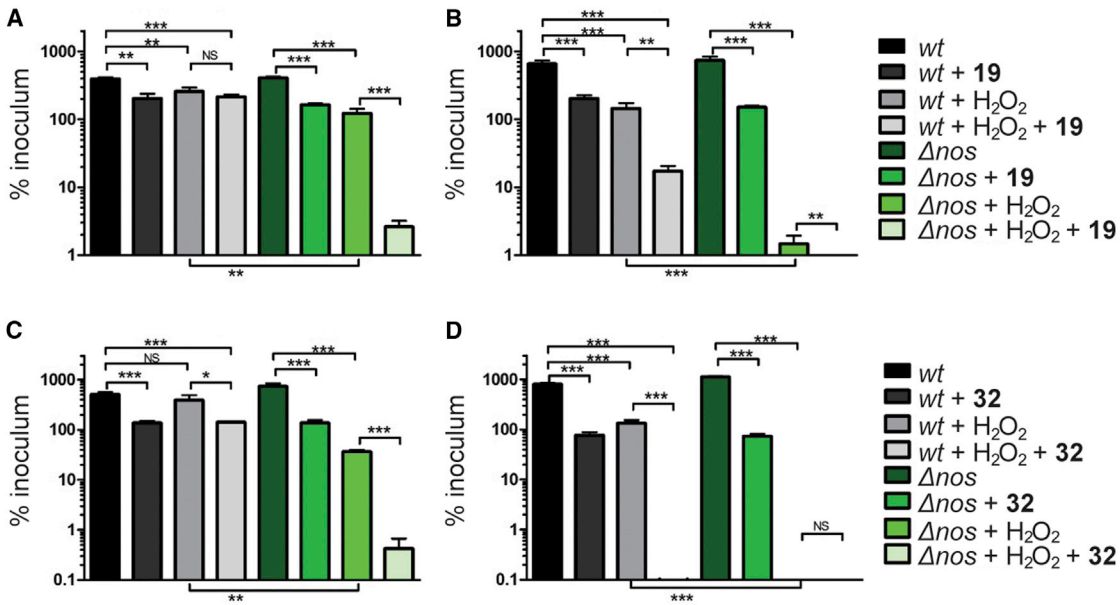

Figure 4. NOS Inhibitors and Peroxide Work Synergistically to Eliminate *S. aureus* over Time

Colonies of *S. aureus* observed after (A) 30 min and (B) 60 min exposure to 200 μM **19** and/or 5 mM H_2O_2. Similarly, *S. aureus* viability was also measured at (C) 30 min and (D) 60 min following exposure to 200 μM **32** and/or 5 mM H_2O_2.

Error bars represent the mean ± SD of three replicates. Student's t test gives ***p < 0.001, **p < 0.01, and *p < 0.05. wt, wild-type.

were cultured in cation-adjusted Mueller-Hinton broth (CAMHB). Prior to H_2O_2 assays, strains were cultured overnight at 37°C and subcultured at a 1/20 dilution in fresh CAMHB. Strains were grown to mid-log phase (OD_{600} ~0.4), pelleted by centrifugation, washed twice in CAMHB, and diluted in CAMHB to a pre-determined concentration approximating 2 × 10^7 cfu/ml. Volumes of 25 μl (5 × 10^5 cfu) were dispensed to 96-well plates (Corning Life Sciences) in 200-μl aliquots of CAMHB and CAMHB with amendments including 5 mM H_2O_2 (Sigma), 200 μM **19**, 200 μM **32**, and equivalent control volumes of **19**/**32** solvent. Plates were incubated at 37°C with shaking. Cultures were sampled at 30-min intervals by removing 25 μl for serial dilution in CAMHB and spot plating on Todd Hewitt agar (Becton Dickinson). Plates were incubated overnight and culture cfu/ml was calculated by enumerating counted colonies and multiplying back through the dilution factor. All conditions were sampled in triplicate; values presented are mean ± SD. Statistical analysis was performed in Excel (Microsoft) using the Student t test.

NOS Inhibitor Cytotoxicity in Mammalian Cell Culture

Cell toxicity assays were performed on mouse embryonic fibroblasts (MEF), which were maintained in DMEM (Corning Cell Gro) media supplemented with 10% fetal calf serum (Sigma-Aldrich) and 1% penicillin-streptomycin (Mediatech, Corning) at ~70% confluency. Cell Titer Glo assays (Cell Titer Glo Luminescent Cell Viability Assay kit, Promega) were performed in clear-bottom 96-well black-cell culture plates (Greiner Bio-One). After plating at 250 cells/well in a volume of 100 μl, cells were left undisturbed for at least 24 hr before addition of NOS inhibitor. NOS inhibitors **19**, **32**, and L-N^G-nitro-arginine methyl ester (Enzo Life Sciences) were added to the MEFs at 40, 20, 10, 5, 2.5, 1.25, 0.625, and 0.3125 μM. Cells were prepared for analysis 72 hr after NOS inhibitors were added by addition of 10 μl of 0.1% Triton X-100 in PBS with shaking for 1 min at room temperature (RT). Cell Titer Glo lysis reagent (20 μl) was then added followed by 1 min of shaking and a 10-min incubation in the dark at RT. Luminescence was detected using an IVIS imaging system (IVIS Lumina II, PerkinElmer). IC_{50} values were determined using the GraphPad Prism software (GraphPad Software).

Chemical Library Preparation

Since bacterial NOS-selective inhibitors had not yet been identified, we collected a diverse set of NOS inhibitors (**1–25**) from our previous NOS studies (Holden et al., 2013; Huang et al., 2012, 2014; Jing et al., 2014; Kang et al., 2014; Kohanski et al., 2007) as well as several newly synthesized molecules (**26–36**). The collected small-molecule library (**1–36**) was composed of a chemically diverse set of aminopyridine derivatives (aminopyridinyl-2-ethyl, aminopyridinyl-2-benzyl, aminopyridinyl-2-phenyl), 7-azaindoles, thiophene amidines, and 2-aminoquinolines. In general, inhibitors **26**–**36** generally have arylalkyl side chains or an N^1,N^2-dimethylethane-1,2-diamine tail. Chemical syntheses and spectral validation of the NOS inhibitors are included in the Supplemental Information.

Chemical Synthesis

Details of the synthesis are provided in the Supplemental Information.

ACCESSION NUMBERS

Coordinate and structure factor files were deposited in the PDB with the accession codes PDB: 4D7H, 4D7I, 4D7J, and 4D7O.

SUPPLEMENTAL INFORMATION

Supplemental Information includes Supplemental Experimental Procedures, two tables, one figure, and five schemes and can be found with this article online at http://dx.doi.org/10.1016/j.chembiol.2015.05.013.

AUTHOR CONTRIBUTIONS

J.K.H. designed and carried out the crystallographic and enzyme assay experiments; S.K. and M.A.C. did the chemical synthesis in the laboratory of R.B.S.; H.L. assisted with X-ray data collection; D.D. assisted J.K.H. with protein preparation; F.C.B. carried out the MRSA experiments in the laboratory of V.N.; S.G.R. evaluated NOS inhibitor cytotoxicity in the laboratory of A.L.E.; J.K.H. and T.L.P. wrote the paper; V.N. and R.B.S. edited the paper.

ACKNOWLEDGMENTS

This work was supported by NIH grants GM57353 (T.L.P.), GM49725 (R.B.S.), HD071600 (V.N.), and AI057153 (V.N.). We also thank the beamline staff at SSRL and ALS for their assistance during the remote X-ray diffraction data collections.

Received: January 7, 2015
Revised: April 20, 2015
Accepted: May 17, 2015
Published: June 18, 2015

REFERENCES

Adak, S., Aulak, K.S., and Stuehr, D.J. (2002). Direct evidence for nitric oxide production by a nitric-oxide synthase-like protein from *Bacillus subtilis*. J. Biol. Chem. *277*, 16167–16171.

Adams, P.D., Mustyakimov, M., Afonine, P.V., and Langan, P. (2009). Generalized X-ray and neutron crystallographic analysis: more accurate and complete structures for biological macromolecules. Acta Crystallogr. D Biol. Crystallogr. *65*, 567–573.

Battye, T.G., Kontogiannis, L., Johnson, O., Powell, H.R., and Leslie, A.G. (2011). iMOSFLM: a new graphical interface for diffraction-image processing with MOSFLM. Acta Crystallogr. D Biol. Crystallogr. *67*, 271–281.

Bird, L.E., Ren, J., Zhang, J., Foxwell, N., Hawkins, A.R., Charles, I.G., and Stammers, D.K. (2002). Crystal structure of SANOS, a bacterial nitric oxide synthase oxygenase protein from *Staphylococcus aureus*. Structure *10*, 1687–1696.

Chartier, F.J., and Couture, M. (2004). Stability of the heme environment of the nitric oxide synthase from *Staphylococcus aureus* in the absence of pterin cofactor. Biophys. J. *87*, 1939–1950.

Cheng, Y., and Prusoff, W.H. (1973). Relationship between the inhibition constant (K_i) and the concentration of inhibitor which causes 50 per cent inhibition (I_{50}) of an enzymatic reaction. Biochem. Pharmacol. *22*, 3099–3108.

Cinelli, M.A., Li, H., Chreifi, G., Martasek, P., Roman, L.J., Poulos, T.L., and Silverman, R.B. (2014). Simplified 2-aminoquinoline-based scaffold for potent and selective neuronal nitric oxide synthase inhibition. J. Med. Chem. *57*, 1513–1530.

Delker, S.L., Xue, F., Li, H., Jamal, J., Silverman, R.B., and Poulos, T.L. (2010). Role of zinc in isoform-selective inhibitor binding to neuronal nitric oxide synthase. Biochemistry *49*, 10803–10810.

Diekema, D.J., Pfaller, M.A., Schmitz, F.J., Smayevsky, J., Bell, J., Jones, R.N., Beach, M., and Group, S.P. (2001). Survey of infections due to *Staphylococcus* species: frequency of occurrence and antimicrobial susceptibility of isolates collected in the United States, Canada, Latin America, Europe, and the Western Pacific region for the SENTRY Antimicrobial Surveillance Program, 1997-1999. Clin. Infect. Dis. *32* (*Suppl 2*), S114–S132.

Evans, P. (2006). Scaling and assessment of data quality. Acta Crystallogr. D Biol. Crystallogr. *62*, 72–82.

Gardete, S., and Tomasz, A. (2014). Mechanisms of vancomycin resistance in *Staphylococcus aureus*. J. Clin. Invest. *124*, 2836–2840.

Gusarov, I., and Nudler, E. (2005). NO-mediated cytoprotection: instant adaptation to oxidative stress in bacteria. Proc. Natl. Acad. Sci. USA *102*, 13855–13860.

Gusarov, I., Shatalin, K., Starodubtseva, M., and Nudler, E. (2009). Endogenous nitric oxide protects bacteria against a wide spectrum of antibiotics. Science *325*, 1380–1384.

Hannibal, L., Somasundaram, R., Tejero, J., Wilson, A., and Stuehr, D.J. (2011). Influence of heme-thiolate in shaping the catalytic properties of a bacterial nitric-oxide synthase. J. Biol. Chem. *286*, 39224–39235.

Hevel, J.M., White, K.A., and Marletta, M.A. (1991). Purification of the inducible murine macrophage nitric oxide synthase. Identification as a flavoprotein. J. Biol. Chem. *266*, 22789–22791.

Holden, J.K., Li, H., Jing, Q., Kang, S., Richo, J., Silverman, R.B., and Poulos, T.L. (2013). Structural and biological studies on bacterial nitric oxide synthase inhibitors. Proc. Natl. Acad. Sci. USA *110*, 18127–18131.

Holden, J.K., Lim, N., and Poulos, T.L. (2014). Identification of redox partners and development of a novel chimeric bacterial nitric oxide synthase for structure activity analyses. J. Biol. Chem. *289*, 29437–29445.

Holden, J.K., Kang, S., Hollingsworth, S.A., Li, H., Lim, N., Chen, S., Huang, H., Xue, F., Tang, W., Silverman, R.B., et al. (2015). Structure-based design of bacterial nitric oxide synthase inhibitors. J. Med. Chem. *58*, 994–1004.

Huang, H., Ji, H., Li, H., Jing, Q., Labby, K.J., Martasek, P., Roman, L.J., Poulos, T.L., and Silverman, R.B. (2012). Selective monocationic inhibitors of neuronal nitric oxide synthase. Binding mode insights from molecular dynamics simulations. J. Am. Chem. Soc. *134*, 11559–11572.

Huang, H., Li, H., Martasek, P., Roman, L.J., Poulos, T.L., and Silverman, R.B. (2013). Structure-guided design of selective inhibitors of neuronal nitric oxide synthase. J. Med. Chem. *56*, 3024–3032.

Huang, H., Li, H., Yang, S., Chreifi, G., Martasek, P., Roman, L.J., Meyskens, F.L., Poulos, T.L., and Silverman, R.B. (2014). Potent and selective double-headed thiophene-2-carboximidamide inhibitors of neuronal nitric oxide synthase for the treatment of melanoma. J. Med. Chem. *57*, 686–700.

Jevons, M.P., Rolinson, G.N., and Knox, R. (1961). "Celbenin"-resistant Staphylococci. Br. Med. J. *1*, 124–125.

Jing, Q., Li, H., Roman, L.J., Martasek, P., Poulos, T.L., and Silverman, R.B. (2014). Combination of chiral linkers with thiophenecarboximidamide heads to improve the selectivity of inhibitors of neuronal nitric oxide synthase. Bioorg. Med. Chem. Lett. *24*, 4504–4510.

Kabsch, W. (2010). XDS. Acta Crystallogr. D Biol. Crystallogr. *66*, 125–132.

Kang, S., Tang, W., Li, H., Chreifi, G., Martasek, P., Roman, L.J., Poulos, T.L., and Silverman, R.B. (2014). Nitric oxide synthase inhibitors that interact with both heme propionate and tetrahydrobiopterin show high isoform selectivity. J. Med. Chem. *57*, 4382–4396.

Kohanski, M.A., Dwyer, D.J., Hayete, B., Lawrence, C.A., and Collins, J.J. (2007). A common mechanism of cellular death induced by bactericidal antibiotics. Cell *130*, 797–810.

Li, H., Jamal, J., Delker, S., Plaza, C., Ji, H., Jing, Q., Huang, H., Kang, S., Silverman, R.B., and Poulos, T.L. (2014). The mobility of a conserved tyrosine residue controls isoform-dependent enzyme-inhibitor interactions in nitric oxide synthases. Biochemistry *53*, 5272–5279.

Loomba, P.S., Taneja, J., and Mishra, B. (2010). Methicillin and vancomycin resistant *S. aureus* in hospitalized patients. J. Glob. Infect. Dis. *2*, 275–283.

Martasek, P., Miller, R.T., Roman, L.J., Shea, T., and Masters, B.S. (1999). Assay of isoforms of *Escherichia coli*-expressed nitric oxide synthase. Methods Enzymol. *301*, 70–78.

Pant, K., Bilwes, A.M., Adak, S., Stuehr, D.J., and Crane, B.R. (2002). Structure of a nitric oxide synthase heme protein from *Bacillus subtilis*. Biochemistry *41*, 11071–11079.

Reece, S.Y., Woodward, J.J., and Marletta, M.A. (2009). Synthesis of nitric oxide by the NOS-like protein from *Deinococcus radiodurans*: a direct role for tetrahydrofolate. Biochemistry *48*, 5483–5491.

Roman, L.J., Sheta, E.A., Martasek, P., Gross, S.S., Liu, Q., and Masters, B.S. (1995). High-level expression of functional rat neuronal nitric oxide synthase in *Escherichia coli*. Proc. Natl. Acad. Sci. USA *92*, 8428–8432.

Schuttelkopf, A.W., and van Aalten, D.M. (2004). PRODRG: a tool for high-throughput crystallography of protein-ligand complexes. Acta Crystallogr. D Biol. Crystallogr. *60*, 1355–1363.

Shatalin, K., Gusarov, I., Avetissova, E., Shatalina, Y., McQuade, L.E., Lippard, S.J., and Nudler, E. (2008). *Bacillus anthracis*-derived nitric oxide is essential for pathogen virulence and survival in macrophages. Proc. Natl. Acad. Sci. USA *105*, 1009–1013.

Silverman, R.B. (2009). Design of selective neuronal nitric oxide synthase inhibitors for the prevention and treatment of neurodegenerative diseases. Acc. Chem. Res. *42*, 439–451.

Stefani, S., Chung, D.R., Lindsay, J.A., Friedrich, A.W., Kearns, A.M., Westh, H., and Mackenzie, F.M. (2012). Methicillin-resistant *Staphylococcus aureus* (MRSA): global epidemiology and harmonisation of typing methods. Int. J. Antimicrob. Agents *39*, 273–282.

Talbot, G.H., Bradley, J., Edwards, J.E., Jr., Gilbert, D., Scheld, M., Bartlett, J.G., and Antimicrobial Availability Task Force of the Infectious Diseases Society of America. (2006). Bad bugs need drugs: an update on the development pipeline from the Antimicrobial Availability Task Force of the Infectious Diseases Society of America. Clin. Infect. Dis. *42*, 657–668.

Vagin, A.A., Steiner, R.A., Lebedev, A.A., Potterton, L., McNicholas, S., Long, F., and Murshudov, G.N. (2004). REFMAC5 dictionary: organization of prior chemical knowledge and guidelines for its use. Acta Crystallogr. D Biol. Crystallogr. *60*, 2184–2195.

van Sorge, N.M., Beasley, F.C., Gusarov, I., Gonzalez, D.J., von Kockritz-Blickwede, M., Anik, S., Borkowski, A.W., Dorrestein, P.C., Nudler, E., and Nizet, V. (2013). Methicillin-resistant *Staphylococcus aureus* bacterial nitric-oxide synthase affects antibiotic sensitivity and skin abscess development. J. Biol. Chem. *288*, 6417–6426.

Wang, Z.Q., Wei, C.C., Sharma, M., Pant, K., Crane, B.R., and Stuehr, D.J. (2004). A conserved Val to Ile switch near the heme pocket of animal and bacterial nitric-oxide synthases helps determine their distinct catalytic profiles. J. Biol. Chem. *279*, 19018–19025.

Yamamoto, K., Shimamura, K., Sekiguchi, F., and Sunano, S. (2001). Effects of NG-nitro-L-arginine on the blood pressure of spontaneously hypertensive rats with different degrees of hypertension. Clin. Exp. Hypertens. *23*, 533–544.

Yuste, J.E., Echeverry, M.B., Ros-Bernal, F., Gomez, A., Ros, C.M., Campuzano, C.M., Fernandez-Villalba, E., and Herrero, M.T. (2012). 7-Nitroindazole down-regulates dopamine/DARPP-32 signaling in neostriatal neurons in a rat model of Parkinson's disease. Neuropharmacology *63*, 1258–1267.

